ingegneria sismica
International Journal of Earthquake Engineering
Anno XLII – Num.1 - 2025

DYNAMIC RESPONSE AND SEISMIC DESIGN OF STEEL BRIDGES IN COMPLEX ENVIRONMENTS UNDER EARTHQUAKE LOADING

Henry Davidson
Ohio State University, USA

SUMMARY: *To investigate the dynamic response characteristics of steel bridges under seismic loads in complex environments, this paper uses ABAQUS finite element software to establish a three-dimensional structural model of a steel bridge. One synthetic seismic wave and two natural seismic waves (Chalfant Valley and San Fernando) are selected as input to simulate the dynamic response characteristics of the steel bridge along the X and Y axes under different seismic waves. Subsequently, the design of the secondary seismic defense line was completed by installing trans-rubber supports and anti-drop beam devices. The steel structure bridge was reinforced using the method of increasing the cross-sectional area, and its seismic performance was further optimized. The stress of reinforcing bars and concrete under frequent earthquakes and the bending moment at the pier base under rare earthquakes both meet the design requirements. The steel structure bridge designed using the seismic design method in this paper exhibits excellent seismic performance, meets the design requirements for steel structure bridges under different seismic actions, and complies with the seismic design optimization requirements of actual engineering projects.*

KEYWORDS: dynamic response characteristics, finite element, steel structure bridge, seismic wave

1 Introduction

Earthquakes are extremely difficult-to-predict natural disasters characterized by high randomness and significant destructive power. China is located between the Pacific Ring of Fire and the Himalayan-Mediterranean seismic belts, bearing one-third of the world's major continental earthquakes. It is a country prone to earthquake disasters, with frequent occurrences, widespread distribution, high intensity, shallow hypocenters, and severe consequences—one of China's fundamental national conditions [1, 2, 3]. Due to the rugged terrain, bridge engineering plays a crucial role in the highway network of China's earthquake-prone regions [4, 5]. As key nodes in the highway transportation network, bridges are highly susceptible to damage under seismic forces. If an earthquake causes traffic disruption and road paralysis, it will severely hinder subsequent earthquake rescue operations, resulting in immeasurable losses to public safety and the socio-economic sector [6, 7, 8, 9].

It is evident that earthquakes pose a fatal threat to bridge safety. Under the influence of seismic disasters, bridges are prone to damage and even collapse [10, 11]. The stress and de-

*davidson.henry174@gmail.com

formation of bridge structures under seismic loads are two critical indicators for assessing seismic performance, and predicting the seismic dynamic response of structures forms the foundation for seismic design [12, 13, 14]. Meanwhile, to mitigate the impact of earthquakes on bridges, seismic design must be enhanced. Steel structures meet the requirements of seismic design, offering high seismic performance. With the continuous improvement of production technology capabilities, steel structure construction techniques have been significantly refined [15, 16, 17, 18]. In bridge structural design, designers implement a prevention-oriented approach, enhancing the bridge's ability to resist seismic forces as required to ensure structural safety and enable the bridge structure to fully utilize its inherent capabilities [19, 20, 21].

Currently, research on the seismic performance of bridges has covered many aspects, and conducting detailed analyses of seismic responses can help more accurately predict and evaluate the performance of bridges during earthquakes. Gao, Duan, and Qian [22] analyzed the dynamic response of long-span continuous bridges under seismic and load conditions. Using finite element software, a numerical model was established that included the foundation, vehicles, and bridge under inclined seismic waves. By analyzing the train speed and seismic frequency at which the bridge reaches its maximum dynamic response, it was ensured that trains could safely pass over the bridge. Lavorato and Nuti [23] evaluated the seismic performance of reinforced concrete bridges that had been repaired and reinforced. A simulated dynamic testing method was used to measure various indicators of the bridge pier model, providing guidance for the repair and renovation of bridges under seismic loads. Tang, Xie, and Wang [24] explored the residual seismic performance of bridges damaged by earthquakes. A multi-scale hybrid model was used to record the strain response, local deformation, and plastic accumulation of steel arch bridges during earthquake sequences, providing reference opinions for bridge repair work. Li et al. [25] analyzed the dynamic response of long-span cable-stayed bridges under uniform loads and seismic excitation. On one hand, a time-domain analysis framework for the train-bridge system was established. On the other hand, different levels of seismic waves were applied to it. The obtained response results can serve as a reference basis for the safe operation of trains under seismic loads. Xu et al. [26] evaluated the ultimate seismic performance of thin-walled concrete-filled steel tube (CFST) bridge piers. Through quasi-static and quasi-dynamic loading experiments on the established finite element model, it was found that thin-walled CFST bridge piers exhibit low seismic response, while the concrete filling enhances their ultimate seismic capacity. Maleska and Beben [27] investigated the stress conditions of soil-steel composite bridges under seismic excitation using common reinforcement methods, assisting in making rapid, cost-effective, and safe design decisions for traditional bridge alternatives. The aforementioned bridge dynamic response studies not only deepen engineers' understanding of bridge behavior during earthquakes but also provide important guidance and references for engineering practice.

Based on existing bridge damage mechanisms and risk assessment methods, numerous scholars have conducted research on bridge design with high seismic performance. Elmy and Nakamura [28] designed a hybrid structural bridge model composed of rolled steel H-shaped beams and reinforced concrete slabs, while elucidating the load transfer mechanism of the bridge's internal materials. This bridge demonstrated sufficient strength and ductility even under strong seismic forces. Liu et al. [29] considered the seismic performance of bridges under track constraints. By establishing a three-dimensional model integrating the track and bridge components and applying special artificial seismic waves, it was found that the track-bridge interaction enhances the structural integrity of the overall system, enabling effective release of seismic stress under seismic loads. Shen et al. [30] proposed incorporating a new

seismic system into the design of long-span bridges. By combining transverse steel dampers (TSD) with conventional sliding bearings, a reliable load path is provided for the transverse direction of bridge piers, enhancing the bridge's seismic resistance in the transverse direction. Dong et al. [31] developed a self-centering buckling-restrained brace (SC-BRB) structure and applied it to bridge beam-column structures. Nonlinear dynamic analysis results showed that bridges equipped with SC-BRB systems exhibit smaller residual displacements under seismic loads. Wei et al. [32] proposed a bridge-track system design scheme based on energy optimization principles to achieve uniform distribution of hysteretic energy dissipation. The optimized seismic isolation strategy accelerates the energy dissipation distribution of bridge bearings and piers, thereby reducing the dynamic response of the bridge-track system under seismic loads. Park, Chun, and Lee [33] employed a genetic algorithm to optimize the structural design of steel arch bridges made from high-performance bridge steel and traditional rolled steel. This approach not only reduces material costs for steel components but also maintains the dynamic performance of steel bridge structures during seismic analysis. Camacho et al. [34] proposed a reinforced concrete (RC) bridge structural design based on a multi-objective evolutionary algorithm, aiming to extract valuable information from bridge design by balancing material usage, safety performance, and construction costs, ultimately achieving high structural seismic performance. Based on this, selecting appropriate energy-dissipating devices and design schemes for different types of bridges can further enhance their seismic performance.

With advances in metal smelting technology, more high-performance metal materials are being used in bridge construction. However, steel structure bridges, due to their unique pier-beam connection design, have relatively limited options for seismic isolation and vibration reduction design, especially at the transition piers/end piers of the side spans, where the main beams are primarily connected via bearings and blocks. This structural characteristic necessitates special attention to its unique dynamic properties and seismic design when seeking effective vibration reduction measures.

To enhance public safety and the reliability of steel bridge engineering design, this study established a detailed structural model of steel bridges, selected multiple sets of typical seismic waves, and simulated the stress distribution and displacement effects of steel bridges under unidirectional seismic waves in both lateral and longitudinal directions. This approach aimed to identify the weak points of steel bridges and subsequently explore seismic optimization and reinforcement methods for steel bridges. The seismic performance optimization effects of the seismic design strategy proposed in this paper were verified through different scenarios under frequent and rare earthquakes in the case study.

2 Project overview

A steel structure bridge is located at a passenger transport hub in a coastal area, serving as a critical transportation link. The project site is classified as Category II, with a seismic design intensity of 7 degrees. The bridge adopts a steel frame structural system, with a total length of 45.4 meters, a main bridge deck width of 3.8 meters, and a structural height of 6.3 meters. The overall arrangement follows an irregular fan-shaped layout, incorporating two types of columns: steel tubular columns and steel–concrete composite columns. Among these, two steel tubular columns are inclined at an angle of 30.8°.

The bridge deck system is composed of both straight and curved steel beams, including variable-section wedge-shaped beam components. The main load-bearing beams are fabricated using H-section steel. At the staircase location, the bridge deck features a large opening, re-

sulting in a significant variation in planar stiffness, which must be carefully considered in the seismic performance analysis of the structure.

3 Numerical simulation

3.1 Establishment of finite element models

To analyze the dynamic response characteristics and failure mechanisms of steel bridges under seismic loads, a three-dimensional structural model was developed using ABAQUS finite element software. The bottom of the columns was simplified as fixed supports, constraining displacement and rotation in all three directions, expressed as:

$$U_1 = U_2 = U_3 = UR_1 = UR_2 = UR_3 = 0. \tag{1}$$

The steel material was modeled using an ideal elastic–plastic material model, following the Von Mises yield criterion. The Rayleigh damping matrix was used to represent structural damping, expressed as:

$$C = \alpha M + \beta K, \tag{2}$$

where α is the structural mass matrix coefficient and β is the stiffness matrix coefficient. These parameters are determined by the critical damping ratio ξ and the natural frequency of the structure ω. The effects of residual stresses in the steel were neglected, and ideal connections were assumed between components.

3.2 Boundary condition settings

Beam–column joints were modeled as rigid connections, and displacement compatibility was achieved using common nodes. Connections between adjacent members were handled using a master–slave node method, where the constraint equation is:

$$U_m = U_s + R \times \theta. \tag{3}$$

Rayleigh proportional damping was adopted, with a damping ratio of 0.05. Seismic input was applied in the form of acceleration time histories along the two principal horizontal axes (X and Y). To account for the complexity of the structural response, seismic waves were applied independently in each direction, without considering coupling effects between bidirectional excitations. Furthermore, large deformation theory was incorporated in the model to capture geometric nonlinearity, thereby improving the accuracy of the simulation results.

3.3 Material constitutive relations

The numerical simulation of steel structure bridges adopts a bilinear constitutive model to describe the mechanical properties of materials. Steel exhibits linear elastic behavior before yielding, and the stress–strain relationship satisfies Hooke's law $\sigma = E\varepsilon$, where E is the elastic modulus. When the stress exceeds the yield strength σ_y, the material enters the plastic stage. The yield criterion for steel is determined using the Von Mises criterion, with the yield function expressed as:

$$f(\sigma_{ij}) = \sqrt{\frac{(\sigma_1 - \sigma_2)^2 + (\sigma_2 - \sigma_3)^2 + (\sigma_3 - \sigma_1)^2}{2}} - \sigma_y = 0. \tag{4}$$

The equivalent composite material also follows the elastic–plastic constitutive relationship, but its equivalent elastic modulus $E^{'}$ and equivalent yield strength $\sigma_y^{'}$ are:

$$E^{'} = \frac{E_s \cdot A_s}{A} + \alpha \cdot \frac{E_c \cdot A_c}{A}, \tag{5}$$

$$\sigma_y^{'} = \frac{f_y \cdot A_s}{A} + \beta \cdot \frac{f_c \cdot A_c}{A}. \tag{6}$$

3.4 Simplified assumptions for calculation

The main beam and crossbeam are rigidly constrained to coordinate node displacement. The handrail system is simplified as additional mass, with its dynamic effects reflected through mass matrix correction. The simplified bearing model employs spring–damper elements, and the bearing stiffness matrix is:

$$[K_s] = \begin{bmatrix} k_x & 0 & 0 \\ 0 & k_y & 0 \\ 0 & 0 & k_z \end{bmatrix}, \tag{7}$$

where k_x and k_y represent horizontal stiffness, k_z represents vertical stiffness, and the stiffness values are determined by the bearing performance parameters.

The foundation soil is simulated using an equivalent spring system, with spring stiffness k calculated as:

$$k = \alpha \cdot E \cdot \frac{A}{L}, \tag{8}$$

where α is the foundation adjustment coefficient, E is the elastic modulus of the foundation soil, A is the foundation area, and L is the soil layer thickness.

4 Modal analysis

4.1 Analysis of natural vibration characteristics

Based on the established finite element model, modal analysis was performed on steel structure bridges to determine the natural vibration modes and frequencies. The governing equation of structural vibration is:

$$[M]\{\ddot{x}\} + [C]\{\dot{x}\} + [K]\{x\} = \{0\}, \tag{9}$$

where $[M]$ is the structural mass matrix, $[C]$ is the damping matrix, $[K]$ is the stiffness matrix, $\{x\}$ is the displacement vector, $\{\dot{x}\}$ is the velocity vector, and $\{\ddot{x}\}$ is the acceleration vector.

Through eigenvalue calculations, it was found that the first-order mode exhibits overall lateral translation, the second-order mode exhibits longitudinal translation, the third-order mode shows torsional deformation, and the fourth-order mode represents vertical bending. Modal analysis reveals that the structural stiffness distribution is uneven, leading to the early appearance of torsional modes. In particular, the stairwell opening area demonstrates local stiffness variations, resulting in stress concentration. This area should therefore be a primary focus in subsequent seismic design.

4.2 Natural period calculation

The natural period of steel bridges is obtained by solving the characteristic equation:

$$|[K] - \omega^2[M]| = 0. \tag{10}$$

Here, $[K]$ is the structural stiffness matrix, $[M]$ is the mass matrix, and ω is the circular frequency. The relationship between the natural period T and the circular frequency ω is:

$$T = \frac{2\pi}{\omega}. \tag{11}$$

The characteristic equation was solved using the Lanczos iterative method to obtain the natural periods of each mode. The stiffness-to-weight ratio of the structure is denoted as λ and is calculated as:

$$\lambda = \frac{H}{T_1} = \frac{6.1}{0.273} = 22.34, \tag{12}$$

where H is the total height of the structure (in meters). The results indicate that the overall stiffness of the structure meets seismic design requirements. For verification, the Rayleigh ratio method was applied:

$$\omega^2 = \frac{\{\varphi\}^T[K]\{\varphi\}}{\{\varphi\}^T[M]\{\varphi\}}, \tag{13}$$

where $\{\varphi\}$ is the assumed displacement mode vector. Considering the irregularity of the structure, a correction coefficient μ is introduced into the fundamental period calculation:

$$T^{'} = \mu T. \tag{14}$$

Here, μ is the correction coefficient associated with the irregularity of the structural plane.

4.3 Selection of damping parameters

The structural damping parameters were determined based on the Rayleigh proportional damping model by controlling the damping ratio of the main modes. The damping coefficient was calculated using an iterative method to determine the mass ratio coefficient α and stiffness ratio coefficient β. The damper parameters were determined based on the maximum elastic deformation of the component and the target damping ratio, with the damping coefficient set to 2.5×10^5 N•s/m. Subsequent time-history analysis results validated the rationality of the selected damping parameters, with the structure exhibiting excellent energy dissipation performance under seismic loads.

5 Seismic dynamic response calculation

5.1 Seismic wave selection and processing

Seismic waves were selected based on site conditions and structural characteristics, with a total of one artificially synthesized seismic wave and two natural seismic waves selected as inputs.

There are many factors that affect seismic waves, including seismic intensity, source, epicenter distance, site conditions, etc. Real seismic records at the project site are difficult to obtain and random in nature, which increases the difficulty of seismic analysis.

5.2 Artificial seismic wave synthesis

Artificial simulated seismic waves can be obtained by fitting the seismic design response spectrum, which can meet the needs of structural seismic analysis and theoretical research. According to the "Code for Seismic Design of Buildings," the design response spectrum is expressed in the form of an influence coefficient curve. Through repeated iteration and fitting of the design response spectrum in the seismic design code, one artificial seismic wave was obtained. The artificially synthesized seismic wave is shown in Figure 1.

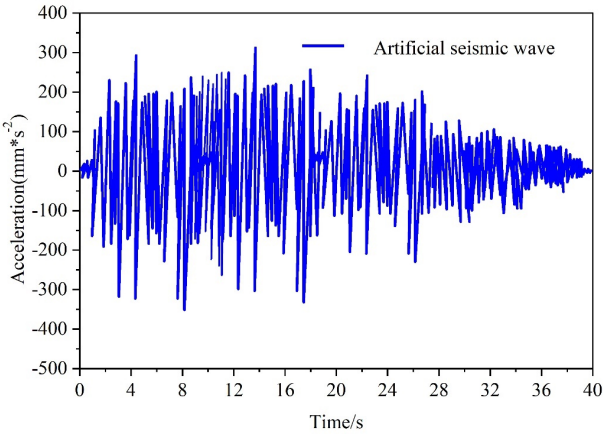

Figure 1: Artificial seismic wave

5.3 Natural seismic wave screening

The selection of seismic waves must consider three factors: spectral characteristics, effective peak values, and duration. Under the influence of different seismic waves, the seismic response of structures varies significantly, making the selection of seismic waves critically important. When selecting seismic waves, factors such as site category, effective peak value, and the fundamental natural vibration periods of the structure in two horizontal directions were fully considered. Two natural seismic waves that met the criteria were selected: the Chalfant Valley wave and the San Fernando wave. These waves satisfy the basic requirements of the code for input seismic waves. The seismic acceleration time history curves of the two natural seismic waves are shown in Figures 2 and 3, respectively.

5.4 Dynamic response time analysis

Dynamic time-history analysis of the steel structure bridge was carried out using the Newmark-β method. An implicit integration format was adopted to ensure numerical stability during the calculations. Three seismic waves were independently applied along the X and Y axes, and the seismic performance of the structure was evaluated by monitoring displacement, velocity, and acceleration responses at key nodes. The results show that the maximum stress in the support system occurred at 18.4 seconds, with a stress magnitude of 223.1 MPa, remaining below the design yield strength of the steel. The maximum displacement was recorded in the end cantilever beam under X-direction seismic action, reaching 26.45 mm, while the inter-story drift angle was 1/285, satisfying code requirements. Local stress concentration appeared in the stair

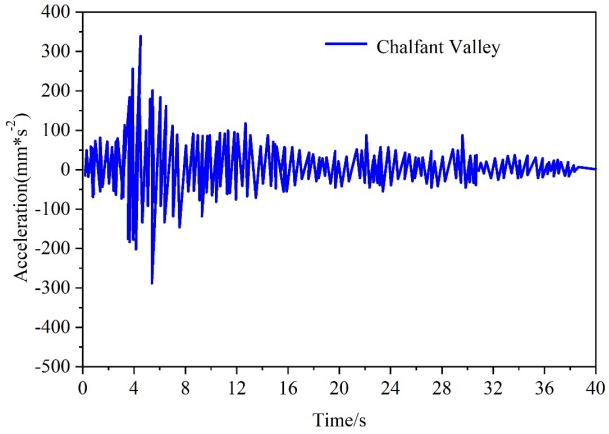

Figure 2: Chalfant valley

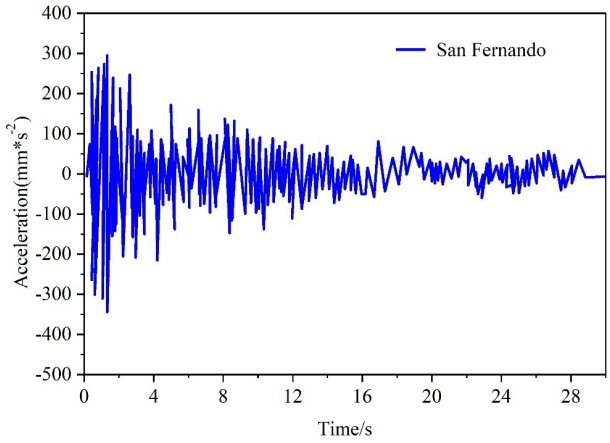

Figure 3: San Fernando

opening area, with a maximum stress of 182.5 MPa, indicating the need for reinforcement measures. Different response characteristics were observed along the two primary axes, with the maximum acceleration response in the Y direction exceeding that in the X direction, reflecting the uneven distribution of stiffness. Numerical simulation confirmed the overall structural stability, with stresses and deformations of key components remaining within allowable limits. The displacement time-history curve revealed a gradual decay of vibrations in the later stages, demonstrating excellent energy dissipation performance of the structure.

5.5 Finite element analysis results

The horizontal seismic dynamic response was evaluated along the two most unfavorable structural directions, namely the transverse (X-axis) and longitudinal (Y-axis) directions. Seismic waves were applied to both axes of the finite element model, and the maximum stress and maximum deflection were calculated to assess the seismic performance of the structure.

5.5.1 Stress response analysis

For artificially generated seismic waves, the stress-time history curves of the steel frame bridge are presented in Figure 4, where (a) and (b) correspond to seismic loads applied along the X-axis

and Y-axis, respectively. Under X-axis excitation, the horizontal supports in the central section of the bridge experienced the maximum stress of 118.0 MPa. Under Y-axis excitation, the maximum stress occurred in the main beam between columns near the passenger terminal, reaching 91.1 MPa. Both values are well below the steel's design strength of 310.0 MPa, confirming the bridge's safety under single-axis seismic loading.

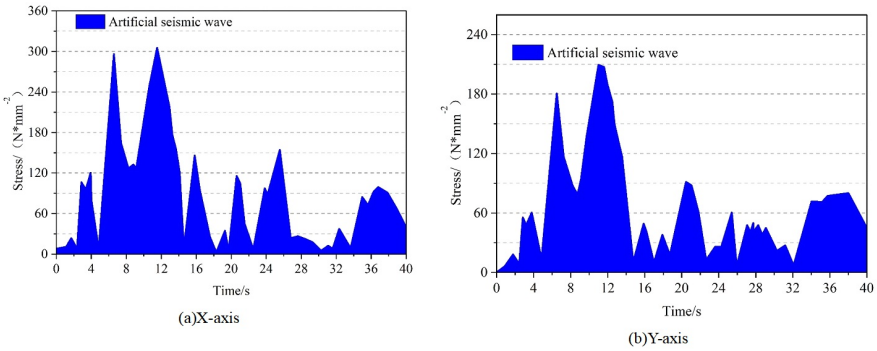

Figure 4: Stress-time curve under artificial seismic waves

During the Chalfant Valley earthquake, the stress responses for the X and Y axes are shown in Figure 5. When subjected to X-axis seismic action, the horizontal support at the bridge's midspan bore the maximum stress of 66.8 MPa. Under Y-axis action, the maximum stress occurred in the main beam between two columns, with a value of 35.1 MPa. Both stress magnitudes are far below the steel's design strength of 310.0 MPa.

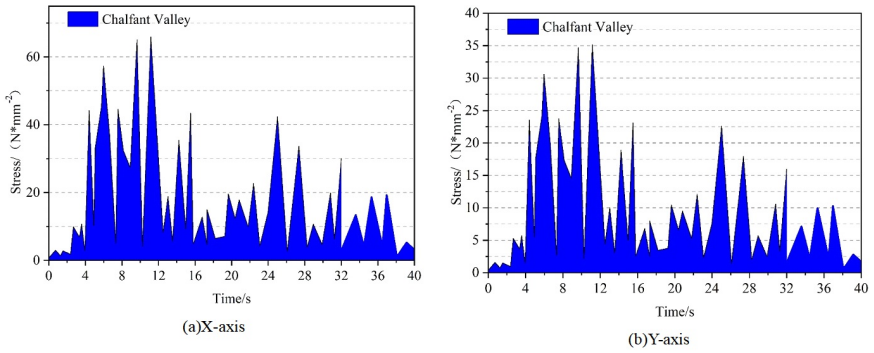

Figure 5: Stress-time curve under Chalfant Valley seismic waves

During the San Fernando earthquake, the structural stress responses along the X and Y axes are illustrated in Figure 6. Under X-axis excitation, the midspan horizontal support experienced a maximum stress of 225.6 MPa. Under Y-axis excitation, the main beam between the columns bore the maximum stress of 118.2 MPa. Both stress values remain within the allowable range, being lower than the steel's design strength of 310.0 MPa.

5.5.2 Displacement response analysis

When subjected to artificially generated seismic waves, the deformation time-history curves of the steel frame bridge are shown in Figure 7, with (a) and (b) representing the results under X-axis and Y-axis seismic loading, respectively. Under X-axis seismic excitation, the maximum displacement occurred at the cantilever beam on the bridge edge, reaching 5.18 mm, which is

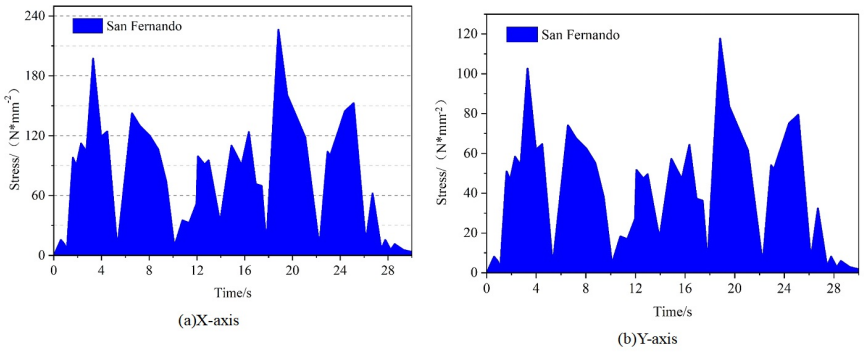

Figure 6: Stress-time curve under San Fernando seismic waves

below the design deflection limit of 7.20 mm. Under Y-axis seismic loading, the maximum displacement occurred at the end cantilever beam, reaching 20.89 mm, also below the design deflection limit of 24.00 mm.

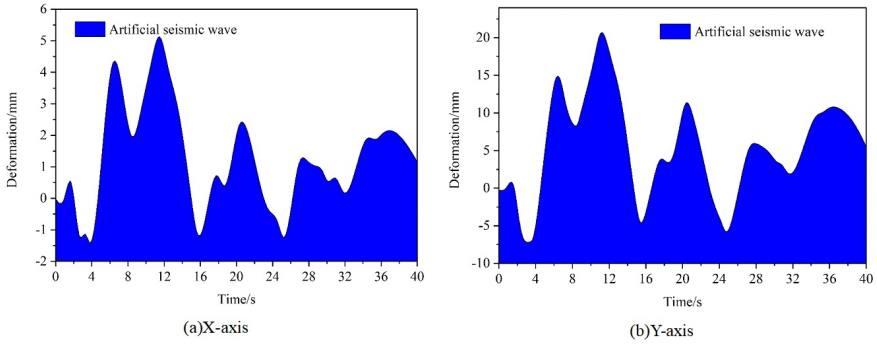

Figure 7: Deformation time-history curve under artificial seismic waves

For the Chalfant Valley earthquake, the seismic response of the bridge along the two principal axes is shown in Figure 8, with (a) and (b) representing the X-axis and Y-axis results, respectively. Under X-axis excitation, the largest displacement was observed at the edge cantilever beam near the bridge center, with a magnitude of 1.76 mm, below the 7.20 mm design limit. Under Y-axis excitation, the end cantilever beam experienced the largest displacement, reaching 7.89 mm, also below the 24.00 mm design limit.

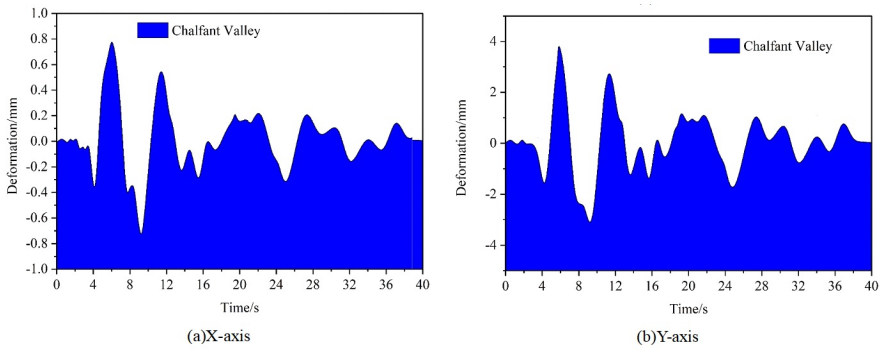

Figure 8: Deformation time-history curve under Chalfant Valley seismic waves

For the San Fernando earthquake, the seismic response results are shown in Figure 9, with

(a) and (b) representing the X-axis and Y-axis results, respectively. The maximum displacements occurred at the edge cantilever beams near the bridge center and at the end cantilever beams, with values of 5.9 mm and 26.95 mm, respectively. Both values remained below their corresponding design limits of 7.20 mm and 24.00 mm.

Across all three seismic wave scenarios, the maximum stresses and deflections of the steel bridge structure did not exceed the limits specified by the "Building Seismic Design Code." Therefore, the results confirm that the bridge is safe under seismic loading and that the structural design scheme is reasonable.

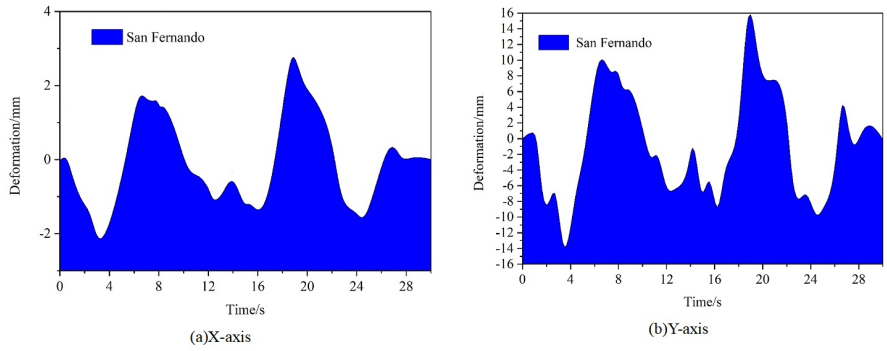

Figure 9: Deformation time-history curve under San Fernando seismic waves

6 Seismic design and reinforcement of steel structure bridges under seismic action

6.1 Seismic design of steel structure bridges

Based on the seismic dynamic response analysis results, a two-level seismic protection strategy was developed for the bridge.

The first-level seismic protection measure involves installing inverted rubber bearings to mitigate sliding displacement during seismic events. These bearings enhance frictional resistance when the bridge experiences lateral movement, thereby reducing deformation. Circular rubber bearings are placed at the bridge–pier connections, using the HFDH400×80 model. The rubber thickness is calculated from the maximum bridge displacement under seismic action according to the formula:

$$e = \frac{2zd}{hq}, \tag{15}$$

where e is the thickness of the rubber bearing, z is the equivalent stiffness under seismic loading, d is the gap between the main beam and pier, and q is the equivalent period corresponding to the maximum displacement.

Based on this calculation, the rubber bearing thickness is 50 mm. Under non-seismic conditions, the bearing remains stationary; during an earthquake, it slides along the friction surface, providing the necessary restraint to limit structural displacement and deformation.

As a second-level seismic defense, anti-falling beam devices are installed below the main beams to prevent collapse during strong ground motions. The design strength of these devices is given by:

$$u = 1.5R, \tag{16}$$

where u is the device design strength and R is the equivalent damping ratio corresponding to the maximum bridge displacement.

The combined implementation of inverted rubber bearings and anti-falling devices ensures that the bridge achieves effective seismic protection, reducing the potential for structural displacement, deformation, and collapse under earthquake action.

6.2 Reinforcement of steel structure bridges

Steel structure bridge connection components can play a supporting role. If the connection components cannot ensure the relative displacement of the upper and lower structures of the bridge, they cannot play a supporting role, posing a major safety hazard to the bridge itself and traffic safety.

6.2.1 Reinforcement of main beams and supports

Currently, the primary methods for reinforcing bridge main beam structures include increasing the cross-sectional area and bonding steel plates. To enhance the seismic resistance of the main beam, reinforcing bars are added to the underside of the beam slab to improve structural ductility, increase the lower interface of the bridge to enhance overall structural performance, and expand the load-bearing area of the beam slab. When reinforcing the underside of the main girder, steel plate bonding is typically employed. The anchorage positions of the steel plates must be clearly defined. When reinforcing the bridge bearings, seismic isolation bearings should be selected or blocks should be used to restrict longitudinal structural displacement, thereby reducing the impact of earthquakes on the bridge structure and preventing the occurrence of girder drop during seismic events.

6.2.2 Reinforcement of abutment and pier structures

The seismic design of the pier section can adopt reinforcement methods that enhance structural ductility. The pier design utilizes steel-concrete structures with hollow cross-sections, and tie beams are installed between transverse pier columns to improve structural connectivity. Based on the load conditions of the pier cap, the diameter of the columns is increased, and denser stirrups are used to enhance the shear resistance of the pier cap structure. Elastic pads are added at the connection points between beams and abutments to reduce structural deformation. The number of piles and columns is increased to enhance the shear resistance of the piers. Seismic damping devices are installed at the ends of the piers to prevent excessive displacement of the upper structure due to excessive bending moments in the lower pier columns, effectively controlling the displacement of tall piers. In this project, the section enlargement method was adopted to reinforce the steel structure bridge. In the entire steel structure bridge, the main beams and piers are the primary compression members. Therefore, the cross-sectional areas of these two components were increased based on the original main beams and piers. Figure 10 shows a schematic diagram of the section enlargement method for reinforcing compression members of the bridge.

Concrete is poured on both sides of the main beam and bridge piers at the bottom. Cement mortar is prepared by mixing cement, water, and lime in a ratio of 2:1:2. The concrete is thoroughly mixed using a concrete mixer, and the mixed concrete is then poured onto the top of the main beam and both sides of the bridge piers using a concrete pump. During the pouring process, use a metal rod to continuously stir the concrete, remove internal air, reduce porosity,

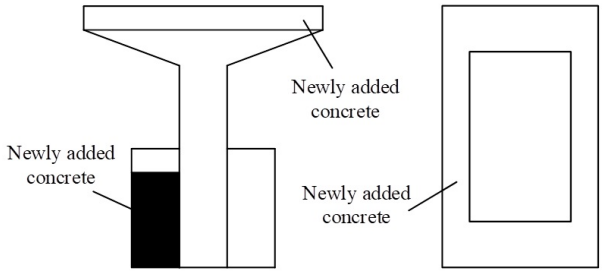

Figure 10: Schematic diagram of reinforcing the compression members of a bridge

and prevent cracks from forming later, which could affect the reinforcement effect. Reinforce the newly added concrete, with a reinforcement ratio controlled between 55% and 58%. The purpose of adding reinforcing bars is to increase the strength of the concrete and enhance the load-bearing capacity of the steel structure bridge's compression members. After the concrete pouring is completed, water is sprayed onto its surface daily, and a layer of wet cotton cloth is placed on top for curing. The curing period is 3 to 5 days. Once curing is complete, normal traffic on the bridge can be resumed, thereby completing the reinforcement of the steel structure bridge.

6.3 Main reinforcement techniques for steel structure bridges

During an earthquake disaster, the most severe form of damage to steel-structured bridges is the failure of the bridge deck under seismic forces. If the bridge deck is damaged, the bridge surface may fracture or collapse, and this could also cause the piers and bearings of the lower structure to fracture. During the reinforcement construction of steel-structured bridges, the following primary reinforcement techniques are commonly employed.

To prevent the bridge from developing significant cracks during an earthquake, the focus of reinforcement should be on enhancing the structural stiffness of the bridge. This can be achieved by employing reinforcement and stabilization steel plate techniques to control the safety range of the bridge's central axis and reinforcement locations.

When reinforcing components, it is essential to ensure that the expansion and contraction performance of the components at the connection points meets technical standards. Reinforcement should be carried out in advance to prevent displacement of critical bridge sections during an earthquake and to avoid the occurrence of propagating cracks.

The proper handling of bridge connection components will significantly impact the bridge's structural continuity and load-bearing capacity. To prevent potential structural cracking at connection points, structural reinforcement between bridge connection components should be implemented to prevent displacement of the connection components.

6.4 Seismic verification

6.4.1 Seismic verification of bridge piers under multiple earthquakes

The overall seismic design principle is to ensure that the structure remains undamaged in minor earthquakes, is repairable in moderate earthquakes, and remains undamaged in major earthquakes. This means that under frequent earthquakes, the structure has a certain strength safety reserve and does not sustain damage. Under rare earthquakes, the structure is allowed to enter the elastic-plastic stage, but it should not collapse.

In Midas Civil, calculations were performed for various conditions, and the most unfavorable internal forces for the portal piers of various steel bridge structures are shown in Table 1. In Table 1, axial forces are negative for compression, with the left column on the left side and the right column on the right side when moving from the smaller mileage to the larger mileage. Based on the results in Table 1, reinforcement calculations were performed. The main reinforcement diameter for the columns is 30 mm, with ordinary reinforcing bars arranged in a single layer at a spacing of 12.0 cm, and prestressed steel strands are installed. The overall reinforcement ratio for the columns is 0.720%. The reinforcement verification results are shown in Table 2. In Table 2, tensile stress is positive, and compressive stress is negative. The stresses in the reinforcing bars and concrete are both less than the design strength of 360 MPa and 19.1 MPa, respectively. Under frequent earthquake actions, the portal piers of steel structure bridges meet the seismic requirements.

Table 1: Internal force Response of stand column under frequent earthquake

Column position	Bridge direction		Cross bridge	
	Axial force /kN	Bending moment /(kN·m)	Axial force /kN	Bending moment /(kN·m)
12#left	-9385.4	22435.5	-7945.6	46658.5
12#right	-19125.6	47158.6	-17724.6	39135.6
13#left	-16542.6	39965.4	-14789.2	40058.1
13#right	-12356.5	28754.9	-10854.3	32054.6
14#left	-15604.8	33456.8	-13545.5	40895.4
14#right	-15478.6	32547.3	-13784.5	26105.2
15#left	-19938.5	47581.5	-18495.2	46845.1
15#right	-13468.5	30245.1	-11755.6	34521.6
18#left	-14584.5	29574.5	-16354.2	49996.2
18#right	-13655.2	30125.4	-11788.8	34215.3

Table 2: Reinforcement checking calculation results

Column position	Bridge direction		Cross bridge	
	Reinforcement bar	Concrete	Reinforcement bar	Concrete
12#left	87.8	-4.9	211.5	-11.7
12#right	192.3	-10.7	138.9	-8.7
13#left	163.0	-9.4	179.2	-9.4
13#right	109.0	-6.6	154.8	-7.5
14#left	110.5	-7.5	189.4	-9.7
14#right	106.4	-7.7	71.3	-5.5
15#left	174.0	-10.8	184.9	-10.7
15#right	104.9	-6.8	156.4	-8.1
18#left	87.5	-6.7	265.1	-11.6
18#right	101.3	-7.0	153.1	-8.1

6.4.2 Seismic verification of bridge piers under rare earthquakes

The most unfavorable internal force responses at the bases of the portal pier columns under rare earthquake actions are shown in Table 3. The bending moment at the pier base is significantly smaller than the equivalent yield bending moment, with the largest difference observed in the

right column of Pier 15, where the bending moment at the pier base is 1,321,892.7 kN·m smaller than the equivalent yield bending moment. Under rare earthquake conditions, the portal piers of steel bridges meet seismic requirements and have sufficient safety reserves.

Table 3: Internal force Response of pier under rare earthquake

Column position	Constant bearing shaft force /kN	The bend of the bridge to the pier /(kN·m)	Cross bridge /(kN·m)	The parallel bridge is the equivalent of the bending moment /(kN·m)
12#left	-8678.3	101511.8	53022.4	115336.5
12#right	-14625.5	77287.6	59112.3	125748.2
13#left	-12548.6	90628.5	52943.6	102085.6
13#right	-10495.96	77978.4	57224.1	98718.4
14#left	-12638.4	87064.5	63394.6	101855.6
14#right	-12536.8	85687.5	47584.2	101722.5
15#left	-20138.5	111244.6	63155.8	141805.6
15#right	-16123.1	86748.1	74451.3	1396344.0
18#left	-10854.6	64418.2	31038.5	99211.5
18#right	-10436.5	41625.3	34665.1	98633.6

7 Conclusion

This paper uses the finite element software ABAQUS to analyze the dynamic response of steel structure bridges under seismic forces in the X and Y principal axes, and optimizes the seismic performance of steel structure bridges through reinforcement.

The stiffness of the X and Y axes of steel structure bridges differs, and under different seismic waves, the weak points of steel structure bridges vary. When seismic waves act on the X-axis, the maximum stress is located on the horizontal supports in the middle of the bridge, and the maximum displacement is located on the cantilever beams at the edges of the steel structure bridge. When different seismic waves act on the Y-axis, the maximum stress is located on the main beams between the columns near the passenger terminal, and the maximum displacement is located on the cantilever beams at the ends of the steel structure bridge. During an earthquake, the horizontal supports in the middle of the steel structure bridge, the side cantilever beams, the main beams between the two columns near the passenger terminal, and the end cantilever beams are the relatively weak points of the steel structure bridge, providing direction for improving the seismic performance of the bridge structure.

The application of the seismic design and reinforcement methods proposed in this paper for steel bridge structures revealed that under frequent earthquakes, the stresses in the reinforcing bars and concrete were significantly lower than the design strength. Under rare earthquakes, the bending moment at the pier base was smaller than the equivalent yield bending moment value. The equivalent yield bending moment of the 15# right column is dozens of times greater than the pier base bending moment, indicating that the steel bridge structures designed using the seismic design methods proposed in this paper exhibit excellent seismic performance and meet the requirements for seismic design optimization in practical applications.

References

[1] Feng, K., Li, Q., & Ellingwood, B. R. (2020). Post-earthquake modelling of transportation networks using an agent-based model. *Structure and Infrastructure Engineering, 16*(11), 1578-1592.

[2] Zhang, M., Yang, X., Li, Y., & Li, G. (2024). Comprehensive Impact Analysis of a Transportation Hub Complex under Earthquake Effects: A Case in China. *Journal of Infrastructure Systems, 30*(4), 04024026.

[3] Argyroudis, S., Mitoulis, S., Kaynia, A. M., & Winter, M. G. (2018). Fragility assessment of transportation infrastructure systems subjected to earthquakes. In *Geotechnical Earthquake Engineering and Soil Dynamics V* (pp. 174-183). Reston, VA: American Society of Civil Engineers.

[4] Yuan, W., Feng, R., & Dang, X. (2018, August). Typical earthquake damage and seismic isolation technology for bridges subjected to near-fault ground motions. In 2018 *International Conference on Engineering Simulation and Intelligent Control* (ESAIC) (pp. 314-318). IEEE.

[5] Lai, Z., Kang, X., Jiang, L., Zhou, W., Feng, Y., Zhang, Y., ... & Nie, L. (2020). Earthquake influence on the rail irregularity on high-speed railway bridge. *Shock and Vibration, 2020*(1), 4315304.

[6] Chen, Z., Han, Z., Zhai, W., & Yang, J. (2019). TMD design for seismic vibration control of high-pier bridges in Sichuan–Tibet Railway and its influence on running trains. *Vehicle System Dynamics, 57*(2), 207-225.

[7] He, X., Wu, T., Zou, Y., Chen, Y. F., Guo, H., & Yu, Z. (2017). Recent developments of high-speed railway bridges in China. *Structure and Infrastructure Engineering, 13*(12), 1584-1595.

[8] Zheng, S. X., Shi, X. H., Jia, H. Y., Zhao, C. H., Qu, H. L., & Shi, X. L. (2020). Seismic response analysis of long-span and asymmetrical suspension bridges subjected to near-fault ground motion. *Engineering Failure Analysis, 115*, 104615.

[9] Abbas, M., Elbaz, K., Shen, S. L., & Chen, J. (2021). Earthquake effects on civil engineering structures and perspective mitigation solutions: a review. *Arabian Journal of Geosciences, 14*(14), 1350.

[10] Liao, K. W., Muto, Y., & Gitomarsono, J. (2018). Reliability analysis of river bridge against scours and earthquakes. *Journal of Performance of Constructed Facilities, 32*(3), 04018017.

[11] Huang, X., Hou, S., Liao, M., & Zhu, Z. (2018). Bearing capacity evaluation and reinforcement analysis of bridge piles under strong earthquake conditions. *KSCE Journal of Civil Engineering, 22*(4), 1295-1303.

[12] Jia, H., Liu, Z., Xu, L., Bai, H., Bi, K., Zhang, C., & Zheng, S. (2023). Dynamic response analyses of long-span cable-stayed bridges subjected to pulse-type ground motions. *Soil Dynamics and Earthquake Engineering, 164*, 107591.

[13] Xin, L., Li, X., Zhang, Z., & Zhao, L. (2019). Seismic behavior of long-span concrete-filled steel tubular arch bridge subjected to near-fault fling-step motions. *Engineering Structures, 180*, 148-159.

[14] Alsultani, R., & Khassaf, S. I. (2022). Nonlinear dynamic response analysis of coastal pile foundation bridge pier subjected to current, wave and earthquake actions: As a model of civilian live. *Resmilitaris, 12*(2), 6133-6148.

[15] Uang, C. M., & Bruneau, M. (2018). State-of-the-art review on seismic design of steel structures. *Journal of Structural Engineering, 144*(4), 03118002.

[16] Nie, J., Wang, J., Gou, S., Zhu, Y., & Fan, J. (2019). Technological development and engineering applications of novel steel-concrete composite structures. *Frontiers of Structural and Civil Engineering, 13*(1), 1-14.

[17] Wujian, Y., Xinxin, T., Zhijian, W., Ping, W., & Lin, K. (2023, April). Seismic response of concrete bridge of Lanzhou-Xinjiang high-speed railway under the near-fault strong earthquake. In *Structures* (Vol. 50, pp. 1416-1428). Elsevier.

[18] Xiang, N., Goto, Y., Alam, M. S., & Li, J. (2021). Effect of bonding or unbonding on seismic behavior of bridge elastomeric bearings: lessons learned from past earthquakes in China and Japan and inspirations for future design. *Advances in Bridge Engineering, 2*(1), 14.

[19] Zhang, Q., & Alam, M. S. (2019). Performance-based seismic design of bridges: a global perspective and critical review of past, present and future directions. *Structure and Infrastructure Engineering, 15*(4), 539-554.

[20] Wen, J., Han, Q., Xie, Y., Du, X., & Zhang, J. (2021). Performance-based seismic design and optimization of damper devices for cable-stayed bridge. *Engineering Structures, 237*, 112043.

[21] Su, J., Wang, J., Li, Z., & Liang, X. (2019). Effect of reinforcement grade and concrete strength on seismic performance of reinforced concrete bridge piers. *Engineering Structures, 198*, 109512.

[22] Gao, X. J., Duan, P. H., & Qian, H. (2020). Dynamic response analysis of long-span continuous bridge considering the effect of train speeds and earthquakes. *International Journal of Structural Stability and Dynamics, 20*(06), 2040013.

[23] Lavorato, D., & Nuti, C. (2015). Pseudo-dynamic tests on reinforced concrete bridges repaired and retrofitted after seismic damage. *Engineering Structures, 94*, 96-112.

[24] Tang, Z., Xie, X., & Wang, T. (2016). Residual seismic performance of steel bridges under earthquake sequence. *Earthquakes and Structures, 11*(4), 649-664.

[25] Li, Y., Zhu, S., Cai, C. S., Yang, C., & Qiang, S. (2016). Dynamic response of railway vehicles running on long-span cable-stayed bridge under uniform seismic excitations. *International Journal of Structural Stability and Dynamics, 16*(05), 1550005.

[26] Xu, Q., Sun, H., Ding, F., & Lyu, F. (2023). Analysis of ultimate seismic performance of thin-walled concrete-filled steel tube bridge piers under dynamic load. *Engineering Structures, 292*, 116544.

[27] Maleska, T., & Beben, D. (2023). Behaviour of soil–steel composite bridges under strong seismic excitation with various boundary conditions. *Materials, 16*(2), 650.

[28] Elmy, M. H., & Nakamura, S. (2017). Static and seismic behaviours of innovative hybrid steel reinforced concrete bridge. *Journal of Constructional Steel Research, 138*, 701-713.

[29] Liu, W., Dai, G., Yu, Z., Chen, Y. F., & He, X. (2018). Interaction between continuous welded rail and long-span steel truss arch bridge of a high-speed railway under seismic action. *Structure and Infrastructure Engineering, 14*(8), 1051-1064.

[30] Shen, X., Wang, X., Ye, Q., & Ye, A. (2017). Seismic performance of transverse steel damper seismic system for long span bridges. *Engineering Structures, 141*, 14-28.

[31] Dong, H., Du, X., Han, Q., Hao, H., Bi, K., & Wang, X. (2017). Performance of an innovative self-centering buckling restrained brace for mitigating seismic responses of bridge structures with double-column piers. *Engineering Structures, 148*, 47-62.

[32] Wei, B., Xiao, B., Tan, H., Yang, Z., Jiang, L., & Yu, Y. (2024). Energy response analysis and seismic isolation strategy optimization of high-speed railway bridge-track system under earthquake action. *Soil Dynamics and Earthquake Engineering, 186*, 108917.

[33] Park, J., Chun, Y. H., & Lee, J. (2016). Optimal design of an arch bridge with high performance steel for bridges using genetic algorithm. *International Journal of Steel Structures, 16*(2), 559-572.

[34] Camacho, V. T., Horta, N., Lopes, M., & Oliveira, C. S. (2020). Optimizing earthquake design of reinforced concrete bridge infrastructures based on evolutionary computation techniques. *Structural and Multidisciplinary Optimization, 61*(3), 1087-1105.